Aerosol Science and Technology, 39:428–436, 2005

ISSN: 0278-6826 print / 1521-7388 online
DOI: 10.1080/027868290953416

A Method for Particle Size Amplification by Water Condensation in a Laminar, Thermally Diffusive Flow

Susanne V. Hering and Mark R. Stolzenburg
Aerosol Dynamics Inc., Berkeley, California

A new method is presented for the enlargement of particle size through condensation of water vapor in a laminar, thermally diffusive flow. The method involves the introduction of an air flow at temperature T_i into a wet-walled tube at a temperature $T_w > T_i$. This approach yields higher supersaturation values than either mixing or cold-walled condensers when operating between the same temperature extremes. Model results for the saturation profiles within the condensing region show that the peak supersaturations are reached along the centerline of the flow, and that the activation efficiency curves are steeper for large temperature differences when the cutpoint diameter is smaller. Experiments conducted with three types of aerosol, oleic acid (a water-insoluble oil), a mixture of oxalic acid and sulfate, and with ambient laboratory aerosol confirmed that condensational growth is achieved with this approach, although experimental cutpoints are somewhat higher than predicted for wettable particles.

INTRODUCTION

The enlargement of particle size through condensational growth is one of the oldest approaches for aerosol measurement. In the nineteenth century Aitken enlarged particles through condensation by means of adiabatic expansion of a saturated air sample, enabling him to count the number of "dust" particles in the air. The twentieth century saw the development of many particle counters based on this principal, including those of Pollak, Vonnegut, and Rich (see McMurry 2000). More recently, condensational growth has been used to enable the collection of particles for chemical analysis (Simon and Dasgupta 1995; Khlystov et al. 1995; Weber et al. 2001) or to permit aerodynamic focusing and concentration of ultrafine particles (Sioutas and Koutrakis 1996; Sioutas et al. 1999; Demokritou et al. 2002).

Condensational growth requires the creation of a region of supersaturation. This can be achieved through adiabatic expansion of a saturated air mass, as in the original instruments of Aitken (1889) and Pollak (1959). It may be done through turbulent mixing, as in the particle counting instruments of Kousaka et al. (1982) and Wang et al. (2002) or the on-line ion chemistry methods cited above. It may also be accomplished through thermal diffusion in a laminar flow, where a saturated airflow is introduced into a cold-walled condenser (Bricard et al. 1976; Agarwal and Sem 1980; Sinclair 1974). This latter approach is commonly used for condensation particle counters (CPCs). The advantages of continuous flow and well-defined activation efficiencies have led to the widespread use of these instruments in many applications. However, they require butanol or another slowly diffusing molecule as the condensing vapor.

For many applications it would be desirable to have a continuous-flow instrument that utilizes water as the condensing vapor and for which the supersaturations can be well defined. A continuous-flow instrument with a well-defined lower cutpoint is needed for coupling to electrical mobility analyzers for particle size distribution measurements. Water-based condensation counters are suitable for measurements in offices, homes, and other inhabited locations. They present less of a problem for operation in clean rooms or aircraft. Water is generally preferred over butanol or other fluids when collecting particles for chemical analysis.

The early instruments of Aitken (1889), Vonnegut (1954), and Rich (1972) used water as the condensing substance, but they were not continuous. Kousaka et al. (1982) introduced a continuous condensation counter based on the turbulent mixing of two saturated airstreams with differing temperatures. With these instruments the supersaturation is a result of the rapid, nonlinear increase of vapor pressure with temperature and may be used with any condensable vapor, including water or alcohol. Similarly, the steam injection methods of the chemical analysis techniques referenced above utilize turbulent mixing and the nonlinear shape of the vapor pressure curve to create supersaturations.

Designers of instruments for measuring the activation spectrum for cloud condensation nuclei (CCN) have long recognized the challenge of creating controlled supersaturations with water vapor. Often these instruments have a cold wall and a warm wall, both saturated with liquid water (e.g., Hudson 1989). Hoppel et al. (1979) and Chuang et al. (2000) describe

Received 30 November 2004; accepted 5 March 2005.
Currently at University of Minnesota, Dept. of Mechanical Engineering, Minneapolis, MN, 55455.
Address correspondence to Susanne V. Hering, Aerosol Dynamics, Inc., 935 Grayson St., Berkeley, CA 94710, USA. E-mail: susanne@aerosol.us

continuous-flow condensation nucleus counters that employ a segmented condenser with alternating hot and cold rings. This approach produces a supersaturation along the centerline of the flow that oscillates slightly about a mean value that is constant in the axial direction. Earlier, Rogers and Squires (1981) constructed a CCN counter with a wet-walled tube whose wall temperature increased in the direction of the flow. As described by Rogers (1977), the centerline supersaturation achieved with this configuration decreases slowly with axial distance, with a larger rate of decrease for higher supersaturations due to the nonlinear characteristics of the supersaturation curve. Recently, Roberts and Nenes (2005) introduced a CCN counter that also utilizes a wet-walled tube with a positive axial temperature gradient, and that addresses issues of buoyancy and flow stability. Leaitch and Megaw (1982), referencing the work of Rogers and Squire, built a somewhat simpler CCN counter that used a warm wet-walled tube held at constant temperature into which a partially saturated airflow was introduced. Leaitch and Megaw report an effective range of supersaturations that could be achieved as 0.04–0.3%. CCN instruments differ from CPCs in that the objective is a well-controlled low supersaturation, rather than the high supersaturations and small-particle activation desired by CPCs.

A new approach for achieving high supersaturations of water vapor in a continuous, laminar flow with subsequent growth of particles through water condensation is described here. The objective is to activate the growth of particles in the nanometer size range, with application to particle number concentration measurement, or low-pressure drop collection of ultrafine particles for chemical analysis. Following the classic work of Vonnegut (1954), this increase in particle diameter through condensation is referred to as "particle size amplification." This article presents the theory and initial experimental validation of this new approach. A companion paper (Hering et al. 2005) describes a commercial condensation particle counter utilizing this method.

THE GROWTH TUBE

The particle size amplifier described here uses a warm, wet-walled "growth tube." Water vapor supersaturation is achieved by introducing air flow into the growth tube, whose temperature is lower than that of the growth tube walls, as illustrated in Figure 1. The walls are actively wetted to maintain a partial pressure of water vapor at the walls near the equilibrium vapor pressure at the wall temperature. The diffusion of water vapor from the walls into the particle-laden stream is faster than the increase in temperature of the particle air stream. This creates a supersaturation along the center line of the growth tube and subsequent particle growth by condensation.

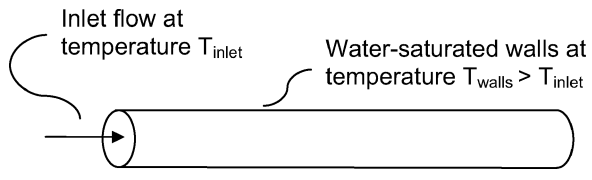

FIG. 1. Schematic of the growth tube, showing a wet-walled tube whose walls are warm with respect to the entering flow.

The geometry is similar to those of prior continuous, laminar-flow condensation counters. The fundamental difference is that the temperature of the walls of our growth tube, which serves as the condenser, is higher than that of the entering air stream. It is also necessary that the walls are wetted. All other high-supersaturation instruments rely on cooling to produce the supersaturation. Instead, the growth tube employs the fact that the mass diffusivity of water vapor exceeds the thermal diffusivity of air. The elevated temperature of the wetted walls produces a high concentration of water vapor, while the "cooling" arises from the entering sample air flow.

ACTIVATION EFFICIENCY

The diameter of the smallest particle that will be activated to take up vapor depends on its chemical composition and upon the saturation ratio, S, defined as the ratio of the partial pressure of the condensing vapor, p_v, to its equilibrium vapor pressure, $p_{sat,T}$, at the flow temperature, T:

$$S = p_v / p_{sat,T}. \quad [1]$$

The smaller the particle the higher the supersaturation required to activate condensational growth. This is because the equilibrium vapor pressure over a droplet is higher than over a flat surface as a result of the droplet surface tension. This effect is described by the Kelvin relation, which associates the equilibrium vapor supersaturation to the diameter of a droplet composed of that condensed vapor, $D_{k,v}$,

$$D_{k,v} = (4\sigma_s M_w)/(\rho_l R_g T \cdot \ln S), \quad [2]$$

where M_w, ρ_l, and σ_s are the molecular weight, liquid density, and surface tension of the condensing species, respectively; R_g is the universal gas constant; and T is the absolute temperature. $D_{k,v}$ is not the activation diameter but instead is a property of the condensing species and is equal to the diameter of a droplet of the condensing species in equilibrium with its vapor at saturation ratio, S, and temperature, T. It is equivalent to the activation diameter for the specific case of a particle that is readily wetted by but insoluble in the condensing vapor. For particles composed of a material that is not wetted by the condensing vapor, the activation diameter will be larger than $D_{k,v}$. For soluble particles, dissolution into the condensate on the particle surface lowers the equilibrium vapor pressure, and the critical diameter required for particle growth is smaller, as described by the Raoult term in the Köhler (1921) equation.

While high supersaturation ratios are desired to activate the smallest particles, very high supersaturation values lead to new particle formation through homogeneous nucleation. This places a practical limit on the smallest particle that can be amplified

through condensational growth. According to classical nucleation theory, the rate of new particle formation is given by

$$N_{Nucl} = \frac{2}{\rho_l}\sqrt{\frac{m_l \sigma_s}{2\pi}}\left(\frac{p_v}{k_B T}\right)^2 \exp\left[-\frac{\pi \sigma_s}{3k_B T} D_{k,v}^2\right], \qquad [3]$$

where m_l is the mass of a vapor molecule and k_B is Boltzmann's constant. Evaluation of Equation (3) shows that for the same temperature and saturation ratio the nucleation rate with butanol is somewhat lower than for water. However, the corresponding value of $D_{k,v}$ is much larger. This is because the quantity $\sigma_s M_w / \rho_l$ that appears in the Kelvin relation in Equation (2) is smaller for water than for butanol by a factor of 1.77. As a result, for the same T and S, $D_{k,v}$ is smaller by a factor of 1.77. At a temperature of 20°C, the onset of nucleation (taken to be $N_{Nucl} > 1$ particle/cm^{3}s) corresponds to a diameter $D_{k,v} = 2.1$ nm for water, while $D_{k,v} = 3.6$ nm for butanol. With butanol systems the temperature at the point of maximum supersaturation is generally lower than for the water system; however, this has a small affect (<2%) on $D_{k,v}$. This analysis indicates that a water-based system could allow detection of smaller particles than the butanol system.

HEAT AND MASS TRANSFER MODELING

The saturation profiles throughout the condensing region are modeled using a two-dimensional model of convective and diffusive heat and mass transfer. For the cylindrical geometry, the values of the temperature, T, throughout the condenser are obtained by solution of the partial differential equation,

$$2U[1-(r/R)^2]\frac{\partial T}{\partial z} = \alpha_t \cdot \frac{1}{r}\frac{\partial}{\partial r}\left(r\frac{\partial T}{\partial r}\right), \qquad [4]$$

where r and z are radial and axial coordinates, respectively; R is tube radius; U is average flow velocity; and α_t is thermal diffusivity of the flowing gas. As in the work of Stolzenburg and McMurry (1991), a fully developed parabolic flow profile is assumed with uniform entering temperature profile and uniform wall temperature. Fluid properties evaluated at a mean temperature are treated as constants over the domain. Axial thermal diffusion (conduction) and other second-order effects such as Stefan flow are ignored.

Profiles of the partial pressure of the water vapor, p_v, are determined by equations analogous to Equation (4) by replacing α_t with vapor diffusivity, α_v. Similarly, particle concentration, $N(D_p)$, (and particle diffusive loss) is determined by replacing α_t with the particle diffusivity, $D(D_p)$. The inlet profiles of vapor pressure and particle concentration are assumed to be uniform; and at the condenser wall the vapor is assumed to be saturated and the particle concentration zero. These three independent boundary value problems each take the form of the classic Graetz problem. Each is solved by separation of variables and each of the three profiles expressed in the form of the standard series solution (see, for example, Eckert and Drake 1972).

COMPARISON TO TRADITIONAL APPROACHES

The difference between our water-based growth tube and the thermally diffusive condensers utilized in the butanol-based CPCs is most easily illustrated through examination of the saturation profiles along the centerline. Under conditions where the parameter $\mu = \alpha\, z/R^2U$ is greater than 0.3, the solution along the centerline to Equation (4) above is represented by the first three terms in the series solution as follows:

$$f = 1.476\exp(-3.657\mu) - 0.806\exp(-22.3\mu) + 0.589\exp(-57\mu). \qquad [5]$$

The temperature along the centerline, T_{cntr}, is obtained from Equation (5) by setting

$$\begin{aligned} \alpha &= \alpha_t = \textit{thermal diffusivity,} \\ \mu &= \mu_t = \alpha_t z/(RU^2), \\ f &= f_T = (T_{cntr} - T_{wall})/(T_{inlet} - T_{wall}), \end{aligned} \qquad [6]$$

where T_{wall} is the temperature of the tube wall and T_{inlet} is the temperature of the entering flow. Similarly, the partial pressure of vapor is also given by Equation (5) with

$$\begin{aligned} \alpha &= \alpha_v = \textit{vapor mass diffusivity,} \\ \mu &= \mu_v = \alpha_v z/(RU^2), \\ f &= f_{p_v} = (p_{v,cntr} - p_{v,wall})/(p_{v,inlet} - p_{v,wall}), \end{aligned} \qquad [7]$$

where $p_{v,cntr}$, $p_{v,wall}$, and $p_{v,inlet}$ refer to the partial pressure of condensing vapor along the centerline, at the tube walls, and in the inlet flow, respectively. The parameters μ_t and μ_v are related to the inverse of the respective Péclet numbers for heat and mass transfer by $\mu = (z/R)Pe^{-1}$.

Figure 2 compares these centerline conditions for butanol- and water-based systems. Shown is the relationship between the vapor pressure and temperature when a warm (40°C), saturated flow is introduced into a cold-walled (10°C) tube (open symbols), and the corresponding relationship when a cold, saturated flow is introduced into a warm-walled tube (solid symbols). The arrows indicate the direction of the change along the flow path. In both cases the tube walls are saturated with the condensing vapor. Also shown is the temperature–vapor pressure relationship for the mixing of two saturated flows at 10°C and 40°C (assuming constant heat capacities). For reference, the dashed line shows the saturation vapor pressure curve.

The $p_v - T$ path followed by the traditional butanol system is shown by the upper line given by the open symbols of Figure 2a. At the entrance of the condenser the flow is saturated at 40°C, and then it follows to the left (to cooler temperatures) along the

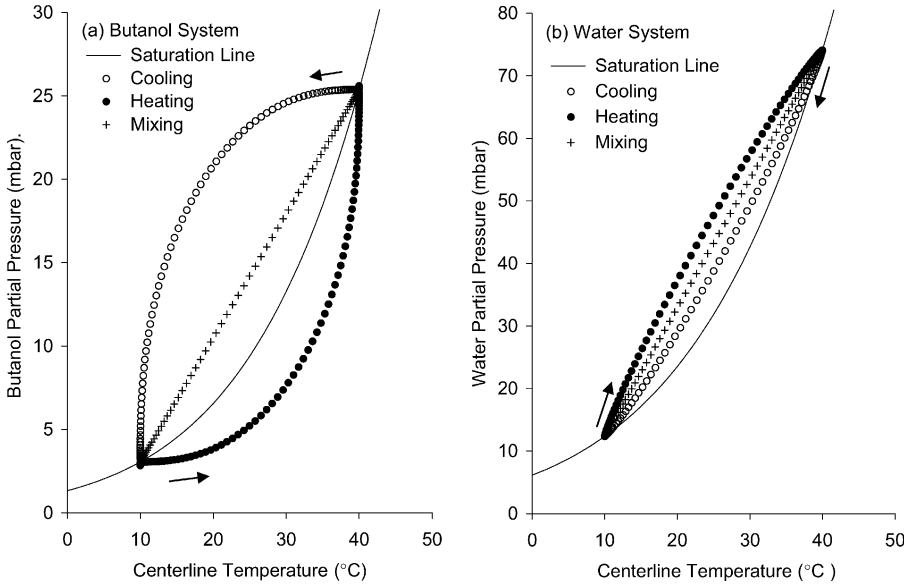

FIG. 2. Comparison of the partial pressure of (a) butanol and (b) water vapor for introduction of a saturated flow into a (○) wet, cold-walled tube or into a (●) wet, warm-walled tube, or for the (+) mixing of saturated flows at differing temperatures. Calculations are for temperature extremes of 10°C and 40°C, respectively (see text).

upper curve. The initial change in the partial pressure of butanol is slow in comparison to the drop in temperature, resulting in partial pressure well in excess of the equilibrium vapor pressure. This is because the mass diffusivity of butanol (0.081 cm^2/s) is much lower than the thermal diffusivity of air (0.215 cm^2/s).

This same approach does not work well with water, which has a vapor mass diffusivity of 0.265 cm^2/s, more than three times higher than that of butanol. When warm, water-vapor-saturated flow is introduced into a cold-walled tube, the centerline vapor pressure changes rapidly, as shown by the lower, open symbols of Figure 2b. As a result, the degree of supersaturation is relatively low, less than that achieved by simple mixing.

An alternate approach is to introduce a cold, water-vapor-saturated flow into a warm, wet-walled tube. The upper solid symbols of Figure 2b, show the temperature–vapor pressure relationship for the introduction of 10°C water-vapor-saturated flow into a wet-walled tube held at 40°C. While this approach does not work for butanol (see the lower, solid symbols of Figure 2a), it is effective for water. In this scenario the diffusion of water vapor from the walls to the centerline is faster than the warming of the flow, and the resulting degree of supersaturation achieved is greater than that for simple mixing. This illustrates the basic principle of the growth tube approach described here.

TEMPERATURE AND SATURATION PROFILES

The radial dependence of temperature and saturation are evaluated in order to assess activation efficiencies for an aerosol flow that fills the growth tube. These are derived from Equation (4) using the first 20 terms of the series solution with their corresponding eigenvalues and eigenfunctions. The water vapor saturation ratio, S, at any point is obtained from the local values of T and p_v in accordance with Equation (1).

Figure 3 shows the axial dependence of S in the growth tube for three different radial positions, $r/R = 0$ (centerline), $r/R = 0.5$, and $r/R = 0.8$. Profiles are shown as a function of the nondimensional parameter defined in Equation (7), namely $\mu_v = \alpha_v z/(RU^2) = \pi\alpha_v(z/Q)$, where we scale with respect to the mass diffusivity of water vapor, and the volumetric flow rate Q. Results are specific to the air–water vapor system but are independent of the tube diameter. The upper graph shows calculations for the growth tube for the case of a saturated air flow at 10°C entering a wet-walled tube at 65°C. Note that the peak supersaturation is reached along the centerline of the flow, with the supersaturation near the walls rapidly decaying to near 1. The lower graph shows what happens with water vapor when the temperatures are reversed, as in the traditional cold-wall condensers. With cold walls the maximum supersaturation achieved is lower, with the largest values occurring near the walls.

Figure 4 shows a contour plot of lines for the growth tube configuration of Figure 3a. Plotted contours correspond to equal values of the parameter $D_{k,v}$ associated with the local saturation ratio and temperature, as given by Equation (2). Because the temperature variation is relatively small, these lines correspond to nearly constant values of the supersaturation, the centerline value of which is shown for each of these contours. The reason for plotting contours of $D_{k,v}$ rather than contours of S is to include the dependence on temperature. Although $D_{k,v}$ is not the activation diameter, the quantity $D_{k,v} \ln S = (4\sigma_s M_w)/(\rho_l R_g T)$ appears in the Köhler relations that describe the activation of soluble particles. As in Figure 3, the radial dimension, r, is normalized with respect to the tube diameter, R, and the axial

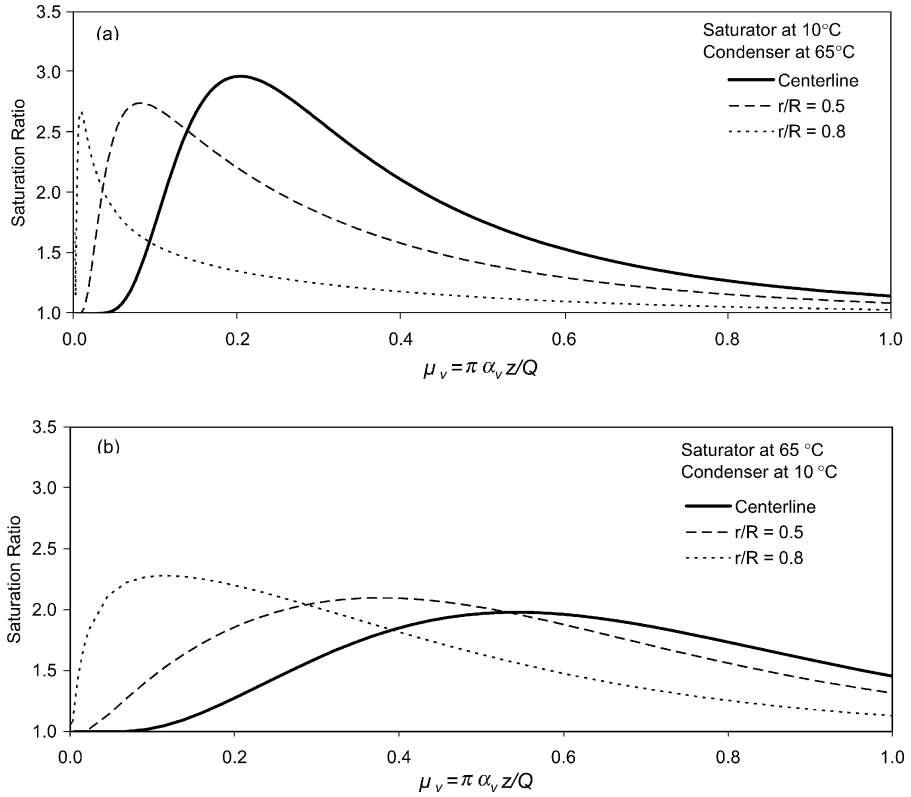

FIG. 3. Axial supersaturation profiles (a) for a saturated flow at 10°C entering a wet-walled tube at 65°C and (b) for a saturated flow at 65°C entering a wet-walled tube at 10°C. The axial dimension z is scaled with the water vapor mass diffusivity, $\alpha_v = 0.265$ cm^2/s, and the volumetric flow rate Q. The radial dimension, r, is expressed in terms of the tube radius, R.

dimension, z, is normalized by $Q/(\pi\alpha_v)$, where α_v is the mass diffusivity of the condensing water vapor. The overall minimum $D_{k,v}$ is located at a point along the centerline. Contours of constant $D_{k,v}$ expand about this point as $D_{k,v}$ increases.

For particles that are not readily wetted by the condensing vapor, the value of S required for activation may be larger than predicted by the Kelvin relation. Similarly, the activation diameter for soluble particles may be smaller than $D_{k,v}$. Yet, for any particle we can define a Kelvin equivalent diameter, $D_{k,eq}$, associated with the saturation ratio, which just activates condensation on the particle. Within the growth tube, particles with diameter $D_{k,eq}$ that pass through a region of supersaturation characterized

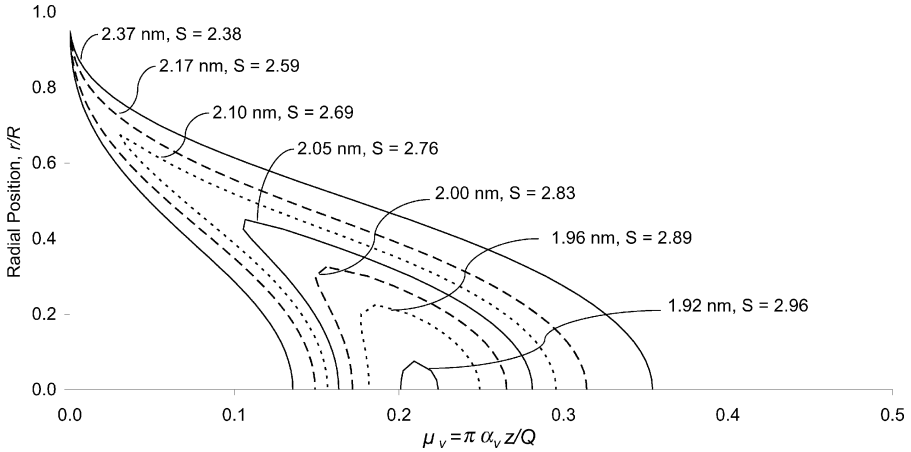

FIG. 4. Lines of equal value of $D_{k,v}$ corresponding to the diameter of water particles in equilibrium with the vapor, as defined by Equation (2), and the peak saturation ratio along the contour. The radial dimension, r, is scaled with respect to the tube radius, R, and the axial dimension, z, is scaled with the water vapor mass diffusivity $\alpha_v = 0.265$ cm^2/s, and the volumetric flow rate, Q .

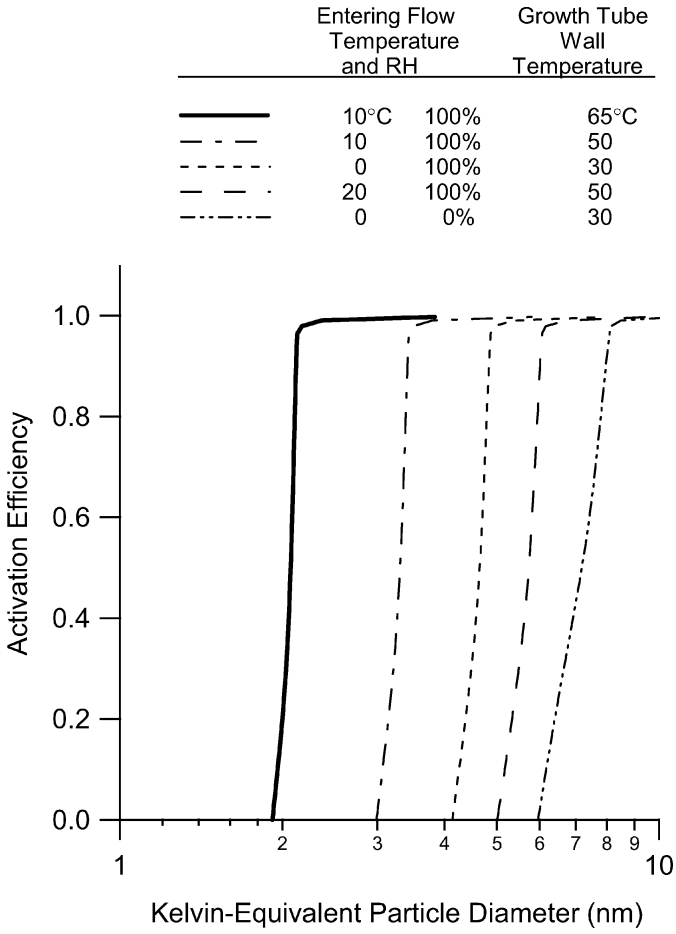

FIG. 5. Activation efficiency from model calculations for flows at varying temperatures and relative humidity entering a warm, wet-walled growth tube.

by $D_{k,v} \leq D_{k,eq}$ are activated, while smaller particles are not. Each $D_{k,v}$ contour extends from the centerline to a point of maximum radial cross section. The activation efficiency is calculated as the fraction of particles of size, $D_{k,eq} = D_{k,v}$, within the maximum radial extent of the $D_{k,v}$ contour. It is found by integrating the Graetz solution for the particle concentration profile, $N(D_p)$, over this cross section.

Figure 5 shows the activation efficiency as a function of the Kelvin-equivalent diameter for five different operating conditions of the growth tube. Generally speaking, the activation is most efficient for large temperature differences between the inlet flow and the wetted walls of the growth tube, and for lower inlet flow temperatures. For a saturated flow at 10°C entering a 65°C growth tube, the cutpoint, corresponding to an activation efficiency of 50%, is at 2.1 nm. The activation cutpoint increases to 3.3 nm when the growth tube temperature is lowered to 50°C. When the temperature difference between the inlet flow and growth tube walls is fixed, as in the curves shown in Figure 5 for inlet temperatures of 0 and 20°C and growth tube temperatures of 30 and 50°C, respectively, the lower inlet flow temperature yields the lower cutpoint (4.7 nm as compared to 5.8 nm). Also, the modeling indicates that there is a significant reduction in the supersaturation when the inlet flow is dry. As shown in Figure 5 for operating temperatures of 0 and 30°C, changing the inlet relative humidity from 100% RH to 0% RH increases the cutpoint from 4.6 nm to 7.2 nm Kelvin-equivalent diameter. The activation efficiency curves are somewhat steeper at the lower cutpoints.

Applications such as condensation particle counting or particle collection require that, once activated, particles grow into the supermicrometer size range so that they may be readily detected or collected. The kinetics of particle growth within the growth tube were examined using the heat and mass transfer relations for the transition regime as given by Fuchs and Sutugin (1971). Calculations were done for temperatures producing peak supersaturations of 1.5 and 1.8. Under these conditions the particle growth is rapid. Particle diameters reach several micrometers within an axial distance of several radii from the point of activation. At fixed volumetric flow rate, the final droplet size is larger when the tube diameter is greater, or the peak supersaturation is higher. Close to the walls the activation occurs sooner and the flow is slower. This provides more time for growth, with the result that the final particle size is comparable to that along the centerline, even though the average supersaturation driving the growth is lower.

Two factors not taken into account by our model are vapor depletion and buoyancy. Vapor depletion is important at high number concentrations. Once some particles are activated, vapor depletion and latent heat release reduce the supersaturation levels downstream, with the effect that small particles are not activated as efficiently. This effect is described theoretically by Metayer et al. (1982) for butanol-based CPCs. Buoyancy effects can be important for large temperature differences if the tube diameter is too large. As pointed out by VanReken et al. (2004) and Roberts and Nenes (2005), this may cause mixing that can degrade the saturation profiles. In our work we took buoyancy into account in the dimensioning of our growth tube used for our experimental investigations described below. This was done by selecting a diameter such that axial pressure gradient due to viscosity is greater than that for buoyancy, i.e., $(8\mu_o Q)/(\pi R^4) > (\rho_{wall} - \rho_{inlet})g$, where μ_o is the air viscosity, Q is the volumetric flow rate, and g is the gravitational constant.

EXPERIMENTAL VERIFICATION

Experimental Methods

Tests were done with a growth tube fabricated from a 6.35 mm ID, 150 mm long porous ceramic tube that was wetted by means of a heated water jacket. The system was unsheathed, that is, all of the flow through the tube contained aerosol. The growth tube was oriented vertically with an upwardly directed flow. A simple optical counter (TSI Model LPC) interfaced directly to the exit of the tube. The lower detection limit of the LPC optical counter is 300 nm. Thus, when particles below the optical detection size pass through the system, they are only counted if they are

activated and grown to at least 300 nm. Experiments were done under two conditions: (1) with a growth tube temperature of 30°C, an inlet flow cooled to 0°C by means of an ice bath, and an air flow of 1.0 l min^{-1}; and (2) a growth tube temperature of 50°C, with the inlet flow at room temperature of 22°C, and an air flow of 0.84 l min^{-1}. In both cases the relative humidity of the entering flow was conditioned to near 100%.

The efficiency of particle activation and growth was determined by reference to a TSI Model 3760 CPC operated in parallel with the growth tube system. The TSI 3760 is a butanol-based CPC with a lower size limit of approximately 15 nm. Efficiencies were determined from the ratio of particle concentration measured by the two systems (the growth tube—LPC and the TSI 3760), corrected for the counting efficiency curve of the TSI 3760 as reported by Wiedensohler et al. (1997). The data of Wiedensohler et al. (1997) extends to 25 nm, for which the TSI 3760 efficiency is 92%. Above this size it was necessary to extrapolate their efficiency data. This was done by linear interpolation to 100% efficiency at 50 nm.

Tests were done with monodisperse fractions of aerosol composed of oleic acid and of an ammonium sulfate and oxalic acid mixture. These were generated by nebulization using alcohol and water solutions for the oleic acid and the sulfate mix, respectively. Particles were size-selected by electrical mobility classification. Tests were also done with mobility-selected fractions of ambient laboratory aerosol. Flow rates were measured with a Gilian bubble flow meter, and temperatures throughout the system were monitored with thermocouples.

RESULTS

Results for particle sizes above 10 nm are shown in Figure 6 for an inlet flow temperature of 0°C and a growth tube temperature of 30°C. Also shown is the efficiency curve for the TSI 3760 that was used in the reduction of the data. Measurements were made for two distinctly different types of aerosols: oleic acid, which is insoluble in water, and a mix of sulfate and oxalic acid, which is both soluble and hygroscopic. With no temperature difference between the growth tube walls and the airflow, only those particles above the nominal lower detection limit of the laser counter are detected. By heating the condenser walls, the counting efficiency is near 100% for all particles above 20 nm. Below this size, the growth tube is somewhat less efficient than the butanol-based TSI 3760 for the water-insoluble (but alcohol-soluble) oleic acid aerosol. Reported concentrations are lower than the TSI 3760 by 30% at 13 nm. For a challenge aerosol of oxalic acid mixed with sulfate, the growth tube system reports concentrations that are higher than those seen by the TSI 3760 by factors of 1.68 and 3.0 for 13 nm and 11 nm, respectively. The growth tube system continued to detect particles at diameters of 7.4 and 8.8 nm, compared to zero counts for the TSI-3760. The data show that for the mixed oxalic acid–ammonium sulfate aerosol the water-based growth tube is more efficient than the

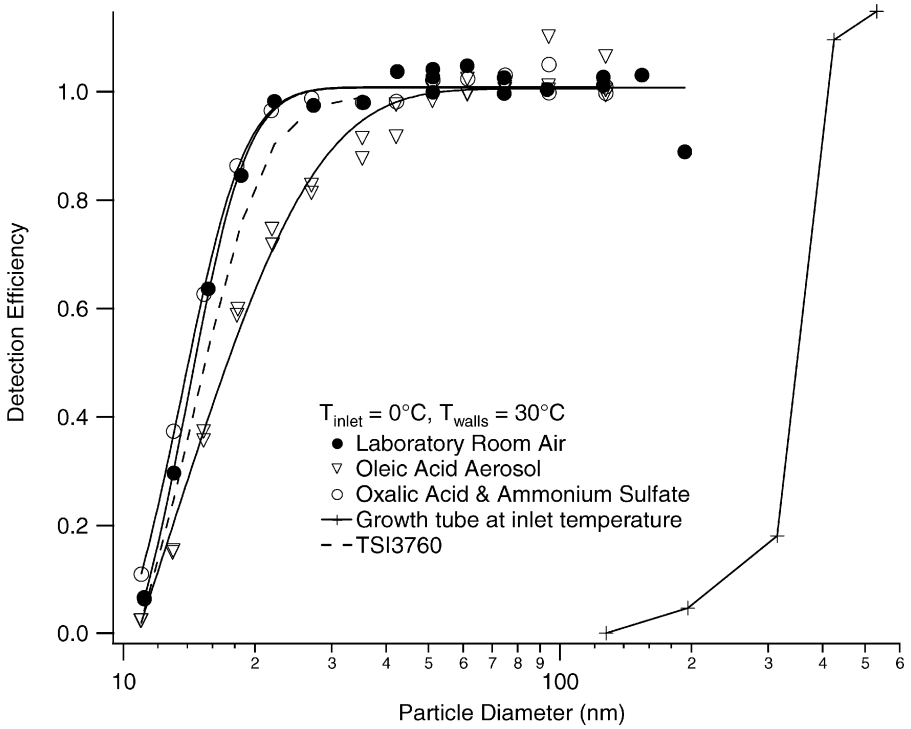

FIG. 6. Detection efficiency as a function of Kelvin equivalent particle diameter for laboratory-generated aerosols of oleic acid and a mix of oxalic acid and ammonium sulfate and for ambient laboratory aerosol for an inlet flow at 0°C, and growth tube temperature of 30°C. Comparison is given to detection when the growth tube was held at the inlet temperature.

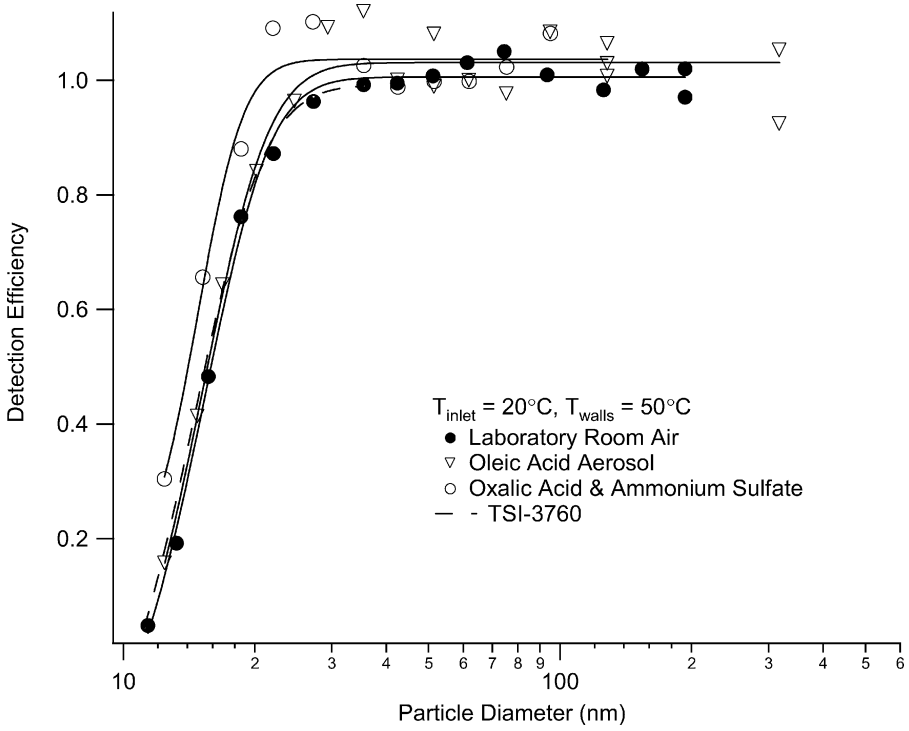

FIG. 7. Detection efficiency as a function of particle diameter for laboratory-generated aerosol of oleic acid, and a mix of oxalic acid and ammonium sulfate, and for ambient laboratory aerosol for an inlet flow at 20°C, and growth tube temperature of 50°C.

butanol-based CPC used as reference. The measured cutpoint is not as small as the predicted $D_{k,v}$value of 5 nm. Nonetheless, there is clear indication of particle growth, enabling particles in the 10 nm size range to be detected optically.

Experiments were also done with inlet flow of 20°C, and a growth tube temperature of 50°C, as shown in Figure 7. Results are similar to those for the 0–30°C system. Again the cutpoint is not as small as the 6 nm predicted activation cutpoint, but the data show that the warm, wet-walled growth tube enables the detection of particles too small to be seen otherwise by the LPC. Differences between the experiment and theory could be due to a number of factors, including difference in temperature between the inside wall of the ceramic tube used for the growth tube and the water jacket where the temperature was measured. Also, accurate assessment of the efficiency was not possible at diameters below 12 nm because of the low counting efficiency in this size range for the TSI 3760 that was used as a reference.

CONCLUSIONS

Presented is the theoretical basis and experimental confirmation of the amplification of particle size through water condensation in a thermally diffusive, laminar flow. The approach involves the introduction of a saturated air flow into a tube with wetted walls held at a temperature greater than that of the entering flow. The theory indicates that activation at particle sizes as small as 2 nm could be achieved with this method. Activation efficiency depends on the absolute temperature as well as the temperature difference between the inlet flow and the growth tube walls. For large temperature differences, corresponding to small cutpoints, the activation efficiency curves are steeper. Experimental data clearly confirm that this approach yields condensational growth of particles. Efficiencies are better for a water-soluble aerosol of oxalic acid mixed with sulfate than for an insoluble nonhygroscopic oil, namely oleic acid.

REFERENCES

Aitken, J. (1889). On the Number of Dust Particles in the Atmosphere, *Proc. Royal Soc. Edinburgh* 26:207–235.

Agarwal, J. K., and Sem, G. J. (1980). Continuous Flow, Single Particle Counting Condensation Nucleus Counter, *J. Aerosol Sci.* 11:343–357.

Bricard, J., Delattre, P., Madelaine, G., and Pourprix, M. (1976). Detection of Ultra-Fine Particles by Means of a Continuous Flux Condensation Nuclei Counter. In *Fine Particles*, edited by B. Y. H. Liu. Academic Press, New York, pp. 565–580.

Chuang, P. Y., Nenes, A., Smith, J. N., Flagan, R. C., and Seinfeld, J. H. (2000). Design of a CCN Instrument for Airborne Measurement, *J. Atmos. Oceanic Technol.* 17:1005–1019.

Demokritou, P., Gupta, T., and Koutrakis, P. (2002). A High Volume Apparatus for the Condensational Growth of Ultrafine Particles for Inhalation Toxicological Studies, *Aerosol Sci. Technol.* 36:1061–1072.

Eckert, E. R. G., and Drake, R. M. (1972). *Analysis of Heat and Mass Transfer*, McGraw-Hill, New York, pp. 333–337.

Fuchs, N. A., and Sutugin, A. (1971). High Dispersed Aerosols. In *Topics in Current Aerosol Research (Part 2)*, edited by G. M. Hidy and J. R. Brock. New York, Pergamon.

Hering, S. V., Stolzenburg, M. R., Quant, F. R., Oberreit, D. R., and Keady, P. B. (2005). A Laminar-Flow, Water-Based Condensation Particle Counter, *Aerosol Sci. Technol.*: in press.

Hoppel, W. A., Twomey, S., and Wojciechowski, T. A. (1979). A Segmented Thermal Diffusion Chamber for Continuous Measurements of CN, *J. Aerosol Sci.* 10:369–373

Hudson, J. (1989). An Instantaneous CCN Spectrometer, *J. Atmos. Oceanic Technol.* 6(6):1055–1065.

Khlystov, A., Wyers, G. P., and Slanina, J. (1995). The Steam-Jet Aerosol Collector, *Atmos. Environ.* 29:2229–2234.

Köhler, H. (1921). Zur kondensation des wasserdampfe in der atmosphäre, *Geofys. Publ.* 2:3–15.

Kousaka, Y., Niida, T., Okuyama, K., and Tanaka, H. (1982). Development of a Mixing Type Condensation Nucleus Counter, *J. Aerosol Sci.* 13:231–240.

Leaitch, R., and Megaw, W. J. (1982). The Diffusion Tube: A Cloud Condensation Nucleus Counter for Use Below 0.3% Supersaturation, *J. Aerosol Sci.* 13:297–319.

McMurry, P. H. (2000). The History of Condensation Nucleus Counters, *Aerosol Sci. Technol.* 33:297–322.

Metayer, Y., Perrin, M. L., and Madelaine, G. (1982). Analysis of Continuous Flow Condensation Nuclei Counter, *J. Aerosol Sci.* 13:170–171.

Pollak, L. W. (1959). Counting of Aitken Nuclei and Applications of the Counting Results, *Int. J. Air Pollut.* 1:293–306.

Rich, T. A. (1972). *Mixing Type Condensation Nuclei Meter*, US Patent 3,694,085.

Roberts, G., and Nenes, A. (2005). A Continuous Flow, Streamwise Thermal Gradient CCN Chamber for Airborne Measurements, *Aerosol Sci. Technol.* accepted.

Rogers, C. F. (1977). A New Device for Studies of Cloud Condensation Nuclei Active at Low Supersaturations, Ph.D. diss. University of Nevada, Reno, University Microfilms, 77-25,082, Ann Arbor, MI.

Rogers, C. F., and Squires, P. (1981). A New Device for Studies of Cloud Condensation Nuclei Active at Low Supersaturations, In *Atmospheric Aerosols and Nuclei, Proceedings of the Ninth international Conference on Atmospheric Aerosols, Condensation and Ice Nuclei, University College Galway Ireland, 21–27 September 1977*, edited by A. F. Roddy and T. C. O'Connor. Galway University Press, Galway, Ireland, pp. 96–100.

Simon, P. K., and Dasgupta, P. K. (1995). Continuous Automated Measurement of the Soluble Fraction of Atmospheric Particulate Matter, *Anal. Chem.* 67:71–78.

Sinclair, D. (1974). *Continuous Flow Condensation Nucleus Counter*, US Patent 3,806,248.

Sioutas, C., Kim, S., and Chang, M. (1999). Development and Evaluation of a Prototype Ultrafine Particle Concentrator, *J. Aerosol Sci.* 30:1001–1017.

Sioutas, C., and Koutrakis, P. (1996). Inertial Separation of Ultrafine Particles Using a Condensational Growth Virtual Impaction System, *Aerosol Sci. Technol.* 25:424–436.

Stolzenburg, M. R., and McMurry, P. H. (1991). An Ultrafine Aerosol Condensation Nucleus Counter, *Aerosol Sci. Technol.* 14:48–65.

VanReken, T. M., Nenes, A., Flagan, R. C., and Seinfeld. J. H. (2004). Concept for a New Cloud Condensation Nucleus (CCN) Spectrometer, *Aerosol Sci. Technol.* 38:639–654.

Vonnegut, B. (1954). *Method and Apparatus for Measuring the Concentration of Condensation Nuclei*, US Patent 2,684,008.

Wang, J., McNeill, V. F., Collins, D. R., and Flagan, R. C. (2002). Fast Mixing Condensation Nucleus Counter: Application to Rapid Scanning Differential Mobility Analyzer Measurements, *Aerosol Sci. Technol.* 36:678–689.

Weber, R. J., Orsini, D., Duan, Y., Lee, Y.-N., Klotz, P. J., and Brechtel, F. (2001). A Particle-Into-Liquid Collector for Rapid Measurement of Aerosol Bulk Chemical Composition, *Aerosol Sci. Technol.* 35:718–727.

Wiedensohler, A., Orsini, D., Covert, D. S., Coffmann, D., Cantrell, W., Havlicek, M., Brechtel, F. J., Russell, L. M., Weber R. J., Gras, J., Hudson, J. G., and Litchy, M. (1997). Intercomparison Study of the Size Dependent Counting Efficiency of 26 Condensation Particle Counters, *Aerosol Sci. Technol.* 27:224–242.